LETTER

https://doi.org/10.1038/s41586-018-0568-2

Crystal structure of a membrane-bound *O*-acyltransferase

Dan Ma[1], Zhizhi Wang[1], Christopher N. Merrikh[2], Kevin S. Lang[2], Peilong Lu[3], Xin Li[1,4], Houra Merrikh[2,5], Zihe Rao[4,6,7,8,9] & Wenqing Xu[1,6]*

Membrane-bound *O*-acyltransferases (MBOATs) are a superfamily of integral transmembrane enzymes that are found in all kingdoms of life[1]. In bacteria, MBOATs modify protective cell-surface polymers. In vertebrates, some MBOAT enzymes—such as acyl-coenzyme A:cholesterol acyltransferase and diacylglycerol acyltransferase 1—are responsible for lipid biosynthesis or phospholipid remodelling[2,3]. Other MBOATs, including porcupine, hedgehog acyltransferase and ghrelin acyltransferase, catalyse essential lipid modifications of secreted proteins such as Wnt, hedgehog and ghrelin, respectively[4–10]. Although many MBOAT proteins are important drug targets, little is known about their molecular architecture and functional mechanisms. Here we present crystal structures of DltB, an MBOAT responsible for the D-alanylation of cell-wall teichoic acid in Gram-positive bacteria[11–16], both alone and in complex with the D-alanyl donor protein DltC. DltB contains a ring of 11 peripheral transmembrane helices, which shield a highly conserved extracellular structural funnel extending into the middle of the lipid bilayer. The conserved catalytic histidine residue is located at the bottom of this funnel and is connected to the intracellular DltC through a narrow tunnel. Mutation of either the catalytic histidine or the DltC-binding site of DltB abolishes the D-alanylation of lipoteichoic acid and sensitizes the Gram-positive bacterium *Bacillus subtilis* to cell-wall stress, which suggests cross-membrane catalysis involving the tunnel. Structure-guided sequence comparison among DltB and vertebrate MBOATs reveals a conserved structural core and suggests that MBOATs from different organisms have similar catalytic mechanisms. Our structures provide a template for understanding structure–function relationships in MBOATs and for developing therapeutic MBOAT inhibitors.

The MBOAT superfamily comprises more than 7,000 proteins (see http://pfam.xfam.org/family/MBOAT). These proteins perform divergent functions with distinct substrate preferences, although many use acyl-coenzyme A (acyl-CoA) as the acyl-group donor (Extended Data Fig. 1). Among bacterial MBOATs, DltB is essential for the D-alanylation of cell-wall teichoic acids[11–16], which are important for the growth, biofilm formation, adhesion and virulence of Gram-positive bacterial pathogens. To understand the molecular mechanisms of MBOAT proteins, we have determined the crystal structure of full-length DltB from *Streptococcus thermophilus* at 3.3 Å resolution (Fig. 1, Extended Data Figs. 2, 3, Extended Data Table 1). DltB contains 415 residues arranged into 17 helices, and both the N and the C termini are located in the extracellular space (Fig. 1a). The helices are located mostly within the lipid bilayer, with the exception of the short N- and C-terminal helices. Among them, 11 transmembrane helices form an external ring-shaped ridge, and shield a central basin that is thinner than the lipid bilayer (Fig. 1, Extended Data Fig. 4). The thin central area results from an intracellular concave surface and a more pronounced extracellular structural funnel (Fig. 1d). Because they are more conserved than the peripheral-ring helices among MBOAT proteins and are probably involved in catalysis (see below), we refer to the structural components in this thin central area as the MBOAT central core. The 3D structure of DltB can be approximately divided into three parts: the N-terminal helical ridge (N-ridge), the central core and the C-terminal helical ridge (C-ridge) (Extended Data Fig. 4). A Dali search using our DltB structure did not find any protein with a similar fold.

The extracellular side of DltB forms a structural funnel, which extends into the middle of the lipid bilayer (Fig. 1d). The surface inside the funnel is formed by residues from several transmembrane helices and loops. Notably, in sharp contrast to the low conservation of residues forming the outer-ridge surfaces, these inner residues are highly conserved among DltB proteins (Fig. 1e, Extended Data Fig. 5). Previous studies have shown that a histidine residue strictly conserved in all confirmed MBOAT proteins is probably involved in catalysis. Mutation of the corresponding histidine residue in all tested MBOATs—porcupine (PORCN), hedgehog acyltransferase (HHAT), ghrelin *O*-acyltransferase (GOAT), diacylglycerol acyltransferase 1 (DGAT1) and acyl-coenzyme A:cholesterol acyltransferase (ACAT)—either abolished or substantially reduced the acyltransferase activities of the enzymes[17–22]. In our DltB structure, this histidine residue (His336, the last residue of helix H14) is located at the bottom of the extracellular funnel (Fig. 1d, f). Another highly conserved histidine residue (His289) in the MBOAT superfamily[1] is also located at the bottom of this funnel and is spatially close to His336 (Extended Data Fig. 3). Our crystal structure and the structural conservation strongly suggest that this extracellular funnel is important for the activity of DltB.

Four *Staphylococcus aureus* DltB mutations—corresponding to *S. thermophilus* DltB mutants S165T, A209D, F250L and F250I—have been identified as resistant to the DltB inhibitors *m*-AMSA (amsacrine) and *o*-AMSA[14]. Ser165, Ala209 and Phe250 are spatially located at the surface of the funnel, with Ser165 and Phe250 sitting near the bottom of the funnel and close to His336 (Fig. 1f). We predict that *m*-AMSA and *o*-AMSA bind in this DltB funnel, and that the abovementioned four mutations may abolish inhibitor binding. We speculate that this funnel may be involved in extracellular teichoic acid substrate binding or have other key roles in catalysis. Given the biological importance of DltB[14] and the marked conservation of the extracellular funnel surface of DltB, inhibitors of DltB that bind to this funnel may act as wide-spectrum antibiotics against Gram-positive bacteria.

In addition to its role in D-alanylation, DltB also has a role in host–pathogen interactions. A missense mutation (T113K) in *S. aureus* DltB is sufficient to convert an *S. aureus* strain from a human-specific pathogen to a rabbit-specific pathogen, without any change in the D-alanylation level of lipoteichoic acid (LTA)[23]. Notably, Thr113—as well as all ten other *S. aureus* DltB residues that are associated with a change in host specificity—is located at a non-conserved extracellular apex (Extended

[1]Department of Biological Structure, University of Washington, Seattle, WA, USA. [2]Department of Microbiology, University of Washington, Seattle, WA, USA. [3]Department of Biochemistry, University of Washington, Seattle, WA, USA. [4]College of Life Sciences, State Key Laboratory of Medicinal Chemistry Laboratory, Nankai University, Tianjin, China. [5]Department of Genome Sciences, University of Washington, Seattle, WA, USA. [6]National Laboratory of Biomacromolecules, CAS Center for Excellence in Biomacromolecules, Institute of Biophysics, Chinese Academy of Sciences, Beijing, China. [7]Shanghai Institute for Advanced Immunochemical Studies, ShanghaiTech University, Shanghai, China. [8]University of Chinese Academy of Sciences, Beijing, China. [9]Laboratory of Structural Biology, School of Medicine, Tsinghua University, Beijing, China. *e-mail: wxu@uw.edu

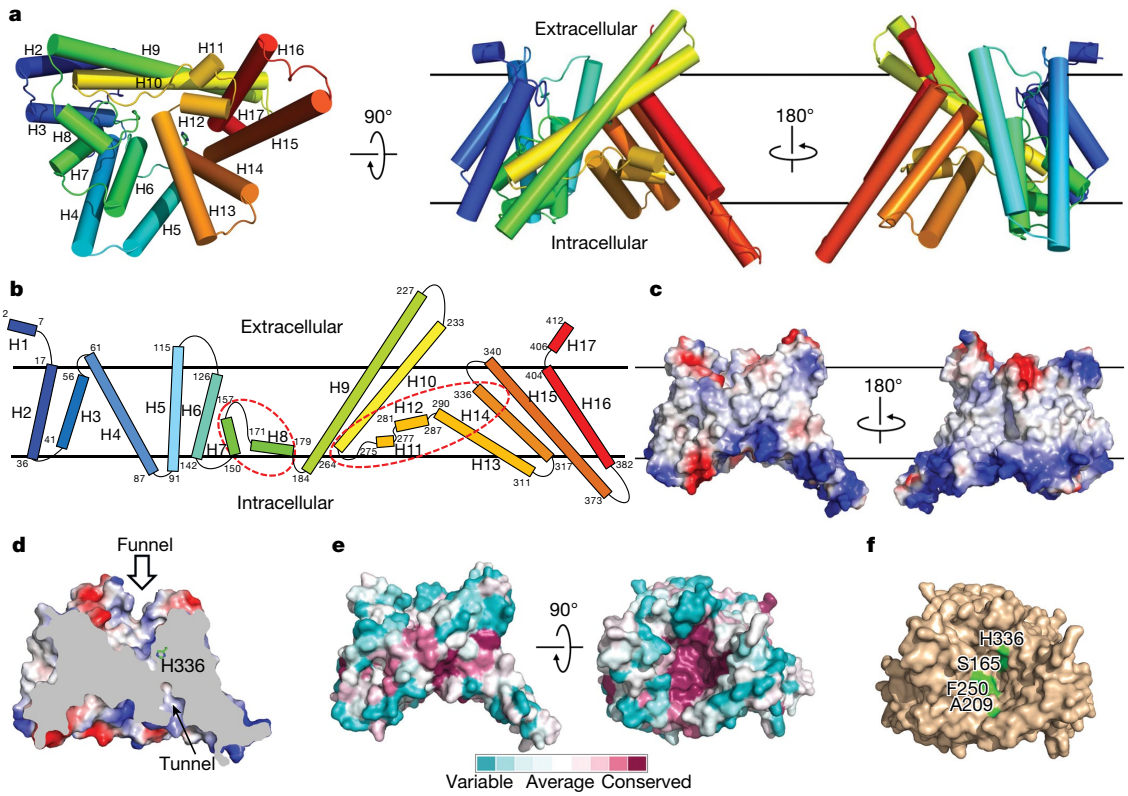

Fig. 1 | Overall structure of DltB and its conserved extracellular funnel. **a**, The DltB crystal structure is shown in three orientations with rainbow colours: bottom, front and back (from left to right). **b**, Cartoon of the transmembrane topology of DltB. DltB contains a ring of 11 peripheral transmembrane helices, which shield a central thin layer (the structural core) highlighted by two red dashed circles. **c**, The electrostatic surface of DltB. **d**, A cut-away surface illustration showing the outward funnel connected with the cytosolic side through a tunnel. The histidine residue that is completely conserved among MBOATs (His336) is located at the bottom of the funnel. **e**, Conservation of the extracellular DltB funnel surface. The surface conservation pattern was generated on the basis of sequence alignment shown in Extended Data Fig. 5. **f**, Top view of DltB showing the location of His336 and the other three DltB residues (Ser165, Ala209 and Phe250) that, when altered, were found to desensitize *S. aureus* to the inhibition of LTA D-alanylation by *m*-AMSA.

Data Figs. 4d, 5). This unusual feature strongly suggests that DltB from *S. aureus* and potentially some other species may interact with one or more unknown host factors using their extracellular ridges.

To serve as the D-alanyl donor to teichoic acid in the Dlt-mediated D-alanylation system, DltC first needs to be modified with the 4′-phosphopantetheine (Ppant) group at Ser35, a modification that can be catalysed by acyl carrier protein synthase (AcpS). The Ppant-modified DltC can be further modified with a D-alanyl group by DltA, through a thioester bond (Fig. 2a). To test whether DltB can directly interact with DltC, we co-expressed His-tagged AcpS and GST-tagged DltC. The purified DltC was uniformly modified by Ppant, as confirmed by mass spectrometry (Extended Data Fig. 2b, c). GST pull-down and size-exclusion chromatography experiments showed that DltC-Ppant and DltB form a tight complex (Fig. 2b). Octet binding analysis showed a K_d of 0.26 μM between DltB and DltC-Ppant (Extended Data Fig. 6). In contrast to the tight DltB–DltC interaction, DltB does not form a detectable complex with DltA or the extracellular domain of DltD, and there is no detectable interaction between DltA and DltC on the cytoplasmic side (data not shown).

To understand how DltB functions as an MBOAT, we also determined the crystal structure of the DltB–DltC-Ppant complex at 3.15 Å resolution (Fig. 2c). Cytoplasmic DltC contains four helices, with Ppant-bonded Ser35 being the first residue of helix 3 (α3). Residues of DltC α3 and the long loop between α3 and α4 (α3–α4 loop) form the DltB-binding surface. DltC interacts mainly with the C-terminal half of DltB H13 and the N-terminal end of DltB H14. This region is formed by a DltB-specific insertion that is missing in other MBOAT proteins[1]. The DltB–DltC interface is mostly hydrophobic, formed by DltB residues Met302, Val305, Ile306 and Met309, and DltC residues Met36, Val39, Val43 and Val55. In addition, Arg317—the first residue of helix H14—forms charged hydrogen bonds with DltC Glu40, whereas the phosphate group of Ser35-Ppant is in a position to form a salt bridge with DltB Lys282 in helix H12 (Fig. 2d, Extended Data Figs. 5, 7). The structures of DltB are essentially identical in both the apo state and the DltC-bound state (Extended Data Fig. 7a).

To confirm the structural and functional features of the DltB–DltC interface, we purified DltB mutants V305D and V305D/I306D as well as DltC mutants V39D and V39R, and tested their interactions with their corresponding wild-type partner using GST pull-down and Octet assays (Fig. 2b, Extended Data Fig. 6). Whereas DltB(V305D) showed substantially reduced binding to wild-type DltC, the binding was completely abolished when using DltB(V305D/I306D). Similarly, both DltC(V39D) and DltC(V39R) showed substantially reduced ability to interact with DltB. These mutagenesis analyses demonstrate that Val305 and Ile306 of DltB and Val39 of DltC are critical to the DltB–DltC interaction, and confirm our structural observation that these surface residues are located at the DltB–DltC core interface.

There is an approximately straight tunnel between the bottom of the extracellular funnel and the cytoplasmic side. This tunnel is formed by three DltB helices from the C-ridge (H13–H15) and the small horizontal helix H12 from the central core. DltB residues inside the tunnel are highly conserved among DltB proteins (Fig. 3a, Extended Data Fig. 5), and show a level of conservation in other MBOAT proteins, which suggests that this tunnel is functionally important. It should be noted that in our current structures of DltB and the DltB–DltC complex, the side chain of the conserved Trp285 from helix H12 keeps this tunnel in a closed conformation (Fig. 3a, Extended Data Fig. 7c). We speculate that the conformation we captured is that of the DltB enzyme in a 'resting' state.

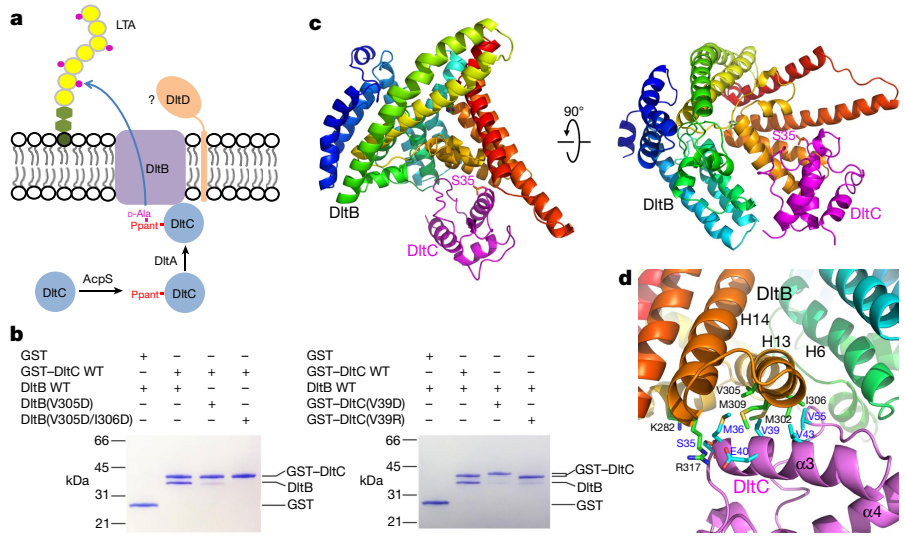

Fig. 2 | Structural basis of the DltB–DltC-Ppant interaction. a, Dlt proteins responsible for LTA D-alanylation in Gram-positive bacteria. The magenta dots on glycerophosphate units represent D-Ala moieties. **b**, Direct stable interaction between DltB and DltC-Ppant, and mutagenesis analysis of the DltB–DltC-Ppant interface, as shown by GST pull-down assays. GST pull-down experiments were performed at least twice with similar results. WT, wild type. **c**, Overall structure of the DltB–DltC-Ppant complex. DltC-Ppant binds to DltB on the cytosolic side, with the phosphate group of Ppant (which is attached through Ser35 of DltC) pointing towards the DltB tunnel. **d**, The DltB–DltC-Ppant interface. Side chains corresponding to DltB are shown as green sticks, and side chains of DltC are shown in cyan.

One notable feature of the DltB–DltC complex is that DltC Ser35 is located at the cytoplasmic entrance of the tunnel (Fig. 3b). Whereas the electron density for the Ppant phosphate group is well-defined in our electron density map, the density for the rest of the Ppant chain is too thin for model building; this is consistent with a 'resting' state conformation. Consistently, Octet analysis showed that the DltC(S35A) mutant can also interact with DltB with similar affinity ($K_d \approx 0.19\,\mu M$) to that of wild-type DltC-Ppant, which indicates that the Ppant group is not essential to the DltB–DltC interaction. The Ppant group can potentially switch between occupying the tunnel and being flexible in the cytoplasmic open space, as the Ser35 phosphate group is positioned between the tunnel entrance and the open cytoplasmic space. While the most conserved residue (His336) is located at the C terminus of the DltB H14 helix, DltC makes contacts with the C-terminal half of the H13 helix and the N terminus of the H14 helix—which suggests that the distance between DltC Ser35 and DltB His336 may be largely fixed during catalysis.

To examine the functional importance of the tunnel, we generated *B. subtilis* strains that lacked the *dlt* operon, and then complemented with a heterologous copy of the *dlt* locus expressed from its native promoter. The LTA D-alanylation level and the viability of *dlt*-deleted *B. subtilis* cells complemented with a heterologous copy of the *dlt* locus, containing either wild-type *dltB* or various *dltB* mutations, were evaluated using ^{14}C- D-Ala radiolabelling and lysozyme-sensitivity

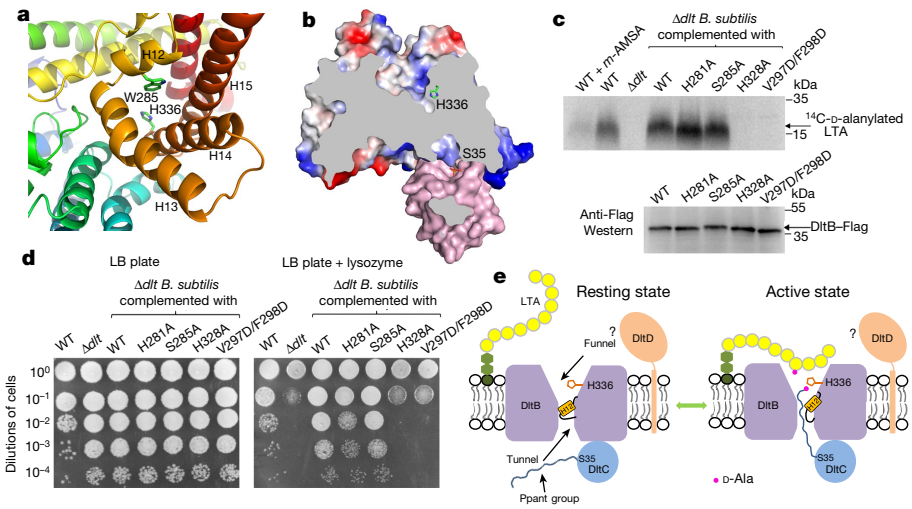

Fig. 3 | Structure of the DltB tunnel and the DltB–DltC-Ppant binding mode provide insight into the molecular mechanism of DltB. **a**, Residues forming the DltB tunnel. **b**, Cut-away surface illustration of the DltB–DltC-Ppant complex. DltC-Ppant pSer35 is located at the bottom of the tunnel. **c**, LTA D-alanylation assay. *m*-AMSA is a DltB inhibitor. The assays were repeated three times. H281, S285, H328 and V297/F298 in *B. subtilis* correspond to H289, S293, H336 and V305/I306 in *S. thermophilus*, respectively. **d**, Lysozyme susceptibility survival assay. Representative images are shown for serial dilutions of cells plated on LB agar (left) and LB agar supplemented with 30 μg ml^{-1} of lysozyme (right). Dilutions of cells are indicated on the *y* axis. The survival assay was performed three times. **e**, A working model for DltB-mediated LTA D-alanylation. Cross-membrane D-alanylation is probably mediated by the DltB tunnel, the opening (activation) of which may be controlled by helix H12. The role of DltD in this reaction is unclear.

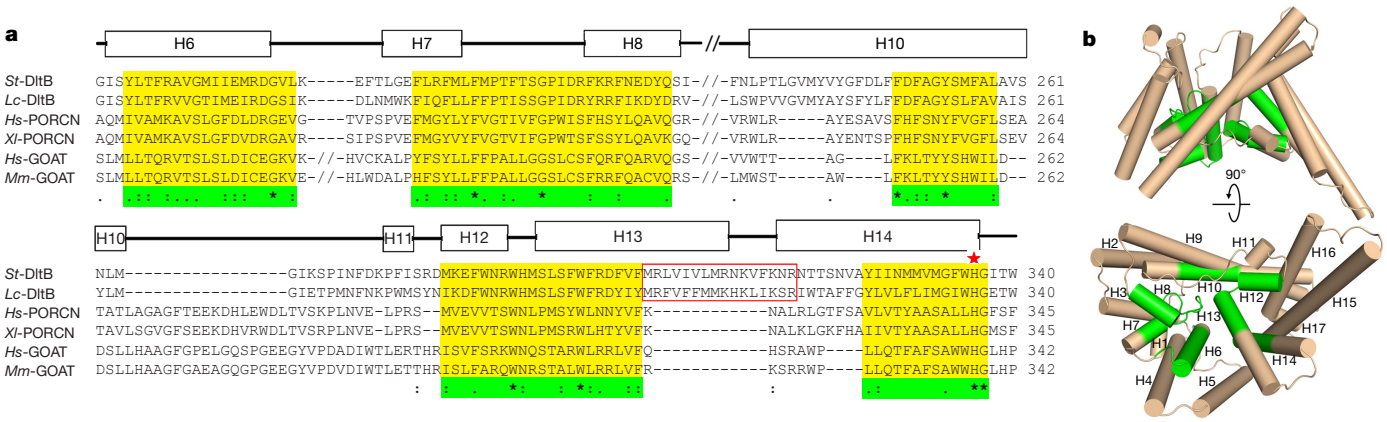

Fig. 4 | Conserved regions among bacterial DltB and vertebrate PORCN and GOAT proteins. a, Alignment of conserved regions of DltB, PORCN and GOAT. Conserved sequences are highlighted in yellow (and in green under the sequences). The red rectangle indicates the DltB-specific insertion, which is involved in the binding of DltC-Ppant. A red star marks the most conserved histidine residue among MBOATs. *St*, *S. thermophilus*; *Lc*, *Lactobacillus casei*; *Hs*, *Homo sapiens*; *Xl*, *Xenopus laevis*; *Mm*, *Mus musculus*. **b**, The conserved MBOAT core. Conserved regions among MBOATs form a central core in the DltB structure (coloured in green), whereas the peripheral helices shielding the core are largely non-conserved (coloured in wheat).

assays, respectively. Mutation of DltB residues corresponding either to *S. thermophilus* DltB His336 or to the DltC-binding site completely abolished LTA D-alanylation (Fig. 3c). In addition, both mutations considerably reduced the viability of *B. subtilis* in the presence of lysozyme, whereas mutations of two other DltB residues did not have a substantial effect in both assays (Fig. 3c, d, Extended Data Fig. 8). Our functional assay data together with the structural features of DltB strongly suggest that the tunnel is important for the catalytic mechanism of DltB (Fig. 3e).

In some other *O*-acyltransferases, such as carnitine acyltransferase[24], a conserved histidine catalyses the acyl-transfer reaction by aligning the carnitine substrate with the acyl-CoA thioester bond. The Ppant- D-Ala chain has a length of around 20 Å between the phosphate group and D-Ala. In our crystal structure, the distance between the Ser35-Ppant phosphate group and His336 is approximately 21 Å. Should the tunnel be open for the Ppant-D-Ala chain binding, this distance would enable His336 to align the substrate that receives the acyl group (probably a glycerol phosphate unit within LTA molecule) with D-alanylated DltC-Ppant. Thus, our structures suggest a model in which D-alanylation of LTA occurs between the LTA bound to the extracellular funnel and the D-alanyl group on DltC-Ppant-D-Ala bound to the cytoplasmic side of the tunnel (Fig. 3e).

Because DltB forms a stable complex with DltC-Ppant even without the D-alanyl group, and the DltC Ser35 is open to the cytosol, we speculate that DltC-Ppant forms a constitutive complex with DltB during catalysis and the Ppant chain can migrate between the tunnel and the cytosol, where loading of the D-alanyl group of DltC-Ppant can be catalysed by DltA. We then asked how the DltB tunnel opens for Ppant binding. The DltB tunnel is formed by the small horizontal helix H12 and the long transmembrane helices (H13–H15) forming the C-ridge of DltB. Compared to the DltB C-ridge helices, helix H12 is more likely to be the mobile structural component. The tunnel opening can be caused by movement or by a conformational change of the short helix H12, the position of which is stabilized through local hydrophobic interactions. H12 may change its position without disturbing the N- and C-ridge structures and lead to the opening of the tunnel. H12 movement may be induced by the presence of an appropriate signal, such as substrate binding with the extracellular funnel and/or binding of intracellular ligands such as DltC-Ppant-D-Ala. It should be noted here that in the Dlt system DltD is required for the D-alanylation of LTA in vivo. It remains unclear how DltD may contribute to this process. A combination of structural and enzymatic analysis is needed to reveal the role of DltD and the detailed catalytic mechanism of DltB.

We next considered the implication of the DltB structure for other MBOAT proteins. Despite a low overall sequence homology, a more conserved region within MBOAT sequences—termed MBOAT2 homology—was identified (http://pfam.xfam.org/family/MBOAT_2). The MBOAT2 homology covers the sequences that correspond to the DltB region from DltB H12 to the N terminus of H15 (Fig. 1b), which forms the majority of the central core that is thinner than the lipid bilayer. Thus, the thin central core and the extracellular (or lumen-facing) funnel are likely to be common structural features in many MBOATs. It has been demonstrated that the most conserved histidine (DltB His336), which is located within this MBOAT2 homology domain, is critical for the enzymatic activities of all tested MBOAT proteins—including PORCN, HHAT, GOAT, ACAT and DGAT[17–22]—which strongly suggests a common or similar catalytic mechanism for the MBOAT superfamily of proteins. The conserved extracellular/lumen structural funnel, the thin central core and the tunnel that we observed in our DltB structure are probably shared by many other MBOATs. Indeed, our crystal structure of DltB is in good agreement with the membrane topology models of HHAT and GOAT that have previously been derived from biochemical data[25–27] (Extended Data Fig. 9). For example, in each case, the catalytic histidine was predicted to be at the end of an HHAT or a GOAT transmembrane helix facing the lumen side, consistent with our structure of DltB. That the critical horizontal helices H11–H13 in our DltB core structure were predicted to be a cytoplasmic subdomain of HHAT or GOAT is also consistent with models. In addition, a predicted 're-entrant helix' observed in both HHAT and GOAT corresponds to the H7–H8 'half-way turn-back' structure in the DltB central core (Fig. 1b, Extended Data Fig. 9). In contrast to the similarity in the core structure, the N- and C-terminal regions of HHAT and GOAT are much more divergent.

Among vertebrate MBOATs, PORCN and GOAT are responsible for lipid modifications of secreted Wnts and ghrelin, respectively. They all catalyse reactions across the endoplasmic reticulum membrane, with the acyl-group-accepting proteins located in the endoplasmic reticulum lumen and acyl-CoA in the cytosol[6,7]. Because DltB also catalyses cross-membrane reactions, we examined the sequence homology among DltB, PORCN and GOAT. It appears that there are four conserved regions: the region covering DltB helices H12–H14 (the MBOAT2 homology region), the DltB H7–H8 region, and two partial helices in the inner circle of the DltB structure (most of helix H6 and the central part of helix H10) (Fig. 4, Extended Data Fig. 9). Therefore, although sequences encoding the N- and C-ridges of DltB are generally not conserved in other MBOATs, the central core of DltB—along with its structural neighbours in the inner circle (for example, parts

of helices H6 and H10)—are conserved among vertebrate MBOATs, including PORCN and GOAT. We suggest that the non-conserved nature of the ridges enable recognition of distinct substrates specific to different members within the MBOAT family. It should be noted that the mechanism of acyl-group binding is probably very different between metazoan MBOATs, most of which bind acyl-CoA as a donor, and DltB, which uses DltC-Ppant-D-Ala.

The deep, conserved DltB extracellular structural funnel, as well as the DltB tunnel, may be an excellent target for drug development. Furthermore, many other bacterial and metazoan MBOATs may also be very druggable targets, as many of them are present on the surface of the cell membrane. In addition, the deep extracellular/lumen funnel shape close to the active site is probably a conserved feature of many MBOATs, and may be an excellent drug-binding site. Indeed, even in the absence of a 3D structure and detailed enzymatic analysis using purified PORCN, multiple small-molecule inhibitors with half-maximal inhibitory concentrations in the low-nanomolar range have been found through cell-based screening, and some of them have been used in clinical trials for the treatment of cancer[28–30]. Potent HHAT and GOAT inhibitors have also been reported and examined in several studies[5]. On the basis of our crystal structures, we predict that many more highly potent MBOAT inhibitors will be discovered in the future.

Three-dimensional structural prediction of MBOAT proteins has been very difficult and unreliable. Our crystal structures of DltB serve as a cornerstone for understanding the structure and function of MBOAT proteins. In addition, our structures reveal an intriguing mechanism for cross-membrane catalysis, and provide a platform for the development of new clinically relevant drugs across species.

Online content

Any methods, additional references, Nature Research reporting summaries, source data, statements of data availability and associated accession codes are available at https://doi.org/10.1038/s41586-018-0568-2.

Received: 11 December 2017; Accepted: 8 August 2018;
Published online 3 October 2018.

1. Hofmann, K. A superfamily of membrane-bound *O*-acyltransferases with implications for Wnt signaling. *Trends Biochem. Sci.* **25**, 111–112 (2000).
2. Chang, T. Y., Chang, C. C., Ohgami, N. & Yamauchi, Y. Cholesterol sensing, trafficking, and esterification. *Annu. Rev. Cell Dev. Biol.* **22**, 129–157 (2006).
3. Liu, Q., Siloto, R. M., Lehner, R., Stone, S. J. & Weselake, R. J. Acyl-CoA:diacylglycerol acyltransferase: molecular biology, biochemistry and biotechnology. *Prog. Lipid Res.* **51**, 350–377 (2012).
4. Chang, S. C. & Magee, A. I. Acyltransferases for secreted signalling proteins (review). *Mol. Membr. Biol.* **26**, 104–113 (2009).
5. Masumoto, N. et al. Membrane bound *O*-acyltransferases and their inhibitors. *Biochem. Soc. Trans.* **43**, 246–252 (2015).
6. Resh, M. D. Fatty acylation of proteins: the long and the short of it. *Prog. Lipid Res.* **63**, 120–131 (2016).
7. Tuladhar, R. & Lum, L. Fatty acyl donor selectivity in membrane bound *O*-acyltransferases and communal cell fate decision-making. *Biochem. Soc. Trans.* **43**, 235–239 (2015).
8. Resh, M. D. Palmitoylation of proteins in cancer. *Biochem. Soc. Trans.* **45**, 409–416 (2017).
9. Lanyon-Hogg, T., Faronato, M., Serwa, R. A. & Tate, E. W. Dynamic protein acylation: new substrates, mechanisms, and drug targets. *Trends Biochem. Sci.* **42**, 566–581 (2017).
10. Madan, B. & Virshup, D. M. Targeting Wnts at the source—new mechanisms, new biomarkers, new drugs. *Mol. Cancer Ther.* **14**, 1087–1094 (2015).
11. Perego, M. et al. Incorporation of D-alanine into lipoteichoic acid and wall teichoic acid in *Bacillus subtilis*. Identification of genes and regulation. *J. Biol. Chem.* **270**, 15598–15606 (1995).
12. Neuhaus, F. C., Heaton, M. P., Debabov, D. V. & Zhang, Q. The *dlt* operon in the biosynthesis of D-alanyl-lipoteichoic acid in *Lactobacillus casei*. *Microb. Drug Resist.* **2**, 77–84 (1996).
13. Reichmann, N. T., Cassona, C. P. & Gründling, A. Revised mechanism of D-alanine incorporation into cell wall polymers in Gram-positive bacteria. *Microbiology* **159**, 1868–1877 (2013).
14. Pasquina, L. et al. A synthetic lethal approach for compound and target identification in *Staphylococcus aureus*. *Nat. Chem. Biol.* **12**, 40–45 (2016).
15. Neuhaus, F. C. & Baddiley, J. A continuum of anionic charge: structures and functions of D-alanyl-teichoic acids in Gram-positive bacteria. *Microbiol. Mol. Biol. Rev.* **67**, 686–723 (2003).
16. Peschel, A. et al. Inactivation of the *dlt* operon in *Staphylococcus aureus* confers sensitivity to defensins, protegrins, and other antimicrobial peptides. *J. Biol. Chem.* **274**, 8405–8410 (1999).
17. Rios-Esteves, J., Haugen, B. & Resh, M. D. Identification of key residues and regions important for porcupine-mediated Wnt acylation. *J. Biol. Chem.* **289**, 17009–17019 (2014).
18. Yang, J., Brown, M. S., Liang, G., Grishin, N. V. & Goldstein, J. L. Identification of the acyltransferase that octanoylates ghrelin, an appetite-stimulating peptide hormone. *Cell* **132**, 387–396 (2008).
19. Buglino, J. A. & Resh, M. D. Identification of conserved regions and residues within hedgehog acyltransferase critical for palmitoylation of sonic hedgehog. *PLoS ONE* **5**, e11195 (2010).
20. Das, A., Davis, M. A. & Rudel, L. L. Identification of putative active site residues of ACAT enzymes. *J. Lipid Res.* **49**, 1770–1781 (2008).
21. Lin, S., Lu, X., Chang, C. C. & Chang, T. Y. Human acyl-coenzyme A:cholesterol acyltransferase expressed in chinese hamster ovary cells: membrane topology and active site location. *Mol. Biol. Cell* **14**, 2447–2460 (2003).
22. McFie, P. J., Stone, S. L., Banman, S. L. & Stone, S. J. Topological orientation of acyl-CoA:diacylglycerol acyltransferase-1 (DGAT1) and identification of a putative active site histidine and the role of the N terminus in dimer/tetramer formation. *J. Biol. Chem.* **285**, 37377–37387 (2010).
23. Viana, D. et al. A single natural nucleotide mutation alters bacterial pathogen host tropism. *Nat. Genet.* **47**, 361–366 (2015).
24. Jogl, G., Hsiao, Y. S. & Tong, L. Structure and function of carnitine acyltransferases. *Ann. NY Acad. Sci.* **1033**, 17–29 (2004).
25. Taylor, M. S. et al. Architectural organization of the metabolic regulatory enzyme ghrelin *O*-acyltransferase. *J. Biol. Chem.* **288**, 32211–32228 (2013).
26. Matevossian, A. & Resh, M. D. Membrane topology of hedgehog acyltransferase. *J. Biol. Chem.* **290**, 2235–2243 (2015).
27. Konitsiotis, A. D. et al. Topological analysis of hedgehog acyltransferase, a multipalmitoylated transmembrane protein. *J. Biol. Chem.* **290**, 3293–3307 (2015).
28. Barnett, B. P. et al. Glucose and weight control in mice with a designed ghrelin *O*-acyltransferase inhibitor. *Science* **330**, 1689–1692 (2010).
29. Ho, S. Y. & Keller, T. H. The use of porcupine inhibitors to target Wnt-driven cancers. *Bioorg. Med. Chem. Lett.* **25**, 5472–5476 (2015).
30. Chen, B. et al. Small molecule-mediated disruption of Wnt-dependent signaling in tissue regeneration and cancer. *Nat. Chem. Biol.* **5**, 100–107 (2009).

Acknowledgements We are grateful to the staff at Advanced Light Source beamlines 5.0.1, 8.2.1 and 8.2.2 for assistance with synchrotron data collection. We thank N. Zheng and P. Hsu for comments on this manuscript, T. Hinds for discussion and advice on assays, S. Ovchinnikov for computational modelling, L. Kruse for use of the radioactive gel scanner and M. Ragheb for construction of the *dlt* operon deletion strain. This work was supported by National Institutes of Health grant R01 GM127316 to W.X. and a Jane Coffin Childs postdoctoral fellowship to D.M. This work was also supported by Chinese Academy of Sciences grant XDB08010303 to Z.R. and W.X., the National Institute of Health grant DP2GM110773 to H.M. and the Bacterial Pathogenesis Training Grant 5T32AI055396-13 to K.S.L.

Reviewer information *Nature* thanks E. Tate and the other anonymous reviewer(s) for their contribution to the peer review of this work.

Author contributions D.M. carried out protein purification, crystallization, and related binding and enzymatic analysis. D.M. and Z.W. collected diffraction data and determined the crystal structure. Z.W. performed structural refinement. C.N.M. constructed the *B. subtilis* strains, and C.N.M., K.S.L. and H.M. performed the cell survival assays. P.L. contributed to molecular cloning and sample preparation. X.L. and Z.R. contributed to screening of other MBOAT proteins. D.M., Z.W. and W.X. analysed structural data and wrote the paper. All authors participated in manuscript revision and analysis of biochemical data.

Competing interests The authors declare no competing interests.

Additional information
Extended data is available for this paper at https://doi.org/10.1038/s41586-018-0568-2.
Supplementary information is available for this paper at https://doi.org/10.1038/s41586-018-0568-2.
Reprints and permissions information is available at http://www.nature.com/reprints.
Correspondence and requests for materials should be addressed to W.X.
Publisher's note: Springer Nature remains neutral with regard to jurisdictional claims in published maps and institutional affiliations.

METHODS

Protein preparation. The cDNA of full-length *S. thermophilus* DltB was subcloned into pET21b (Novagen). cDNAs of *S. thermophilus* AcpS, DltA and DltC were subcloned into pQLink vectors (Addgene) with AcpS and DltA bearing an N-terminal 6×His-tag, and DltC bearing a N-terminal GST-tag. *Escherichia coli* strain C43 (DE3) was used for protein overexpression. Overexpression of the above proteins was induced by 0.4 mM isopropyl β-D-thiogalactoside when cell density reached an optical density at 600 nm (OD_{600}) of 1.0. After induction at 37 °C for 5 h, the cells were collected and homogenized in buffer containing 25 mM Tris-HCl pH 8.0 and 150 mM NaCl.

For DltB purification, after disruption by sonication, cell debris was removed by centrifugation for 10 min at 20,000*g*. The supernatant was collected and ultracentrifuged for 1.5 h at 100,000*g*. The membrane fraction was collected and homogenized with buffer containing 25 mM Tris-HCl pH 8.0 and 150 mM NaCl. *n*-Decyl-β-D-maltopyranoside (Anatrace) was added to the membrane suspension to a final concentration of 1.5% (w/v) and then incubated for 2 h at 4 °C. After another ultracentrifugation step at 100,000*g* for 30 min, the supernatant was collected and loaded onto Ni-NTA affinity resin (Ni-NTA; Qiagen). After washing with buffer containing 25 mM Tris-HCl pH 8.0, 500 mM NaCl, 25 mM imidazole and 0.2% (w/v) *n*-decyl-β-D-maltopyranoside, DltB was eluted with a buffer containing 25 mM Tris-HCl pH 8.0, 150 mM NaCl, 400 mM imidazole and various detergents from Anatrace. After being concentrated to 10 mg ml^{-1}, DltB was further purified by gel filtration (Superdex-200 10/30; GE Healthcare). The buffer for gel filtration contained 25 mM Tris-HCl pH 8.0, 150 mM NaCl and various detergents. The peak fractions were collected.

For the purification of DltA and DltC, after sonication the cell debris was removed by centrifugation for 1 h at 35,000*g*. The supernatants were loaded onto Ni-NTA affinity resin and Glutathione Sepharose 4 resin (GS4B resin, GE Healthcare), respectively. After a wash step, the N-terminal GST-tag was either removed from DltC or maintained, depending on the purpose of the experiment. After elution, DltA and DltC solutions were loaded onto HiTrap Q HP columns (5 ml, GE Healthcare), and protein samples eluted from the Q column were further purified by gel filtration. Peak fractions were collected and concentrated. Finally, DltA and DltC were stored in buffer containing 25 mM Tris-HCl pH 8.0 and 150 mM NaCl.

DltB and DltC mutants were generated with a standard PCR-based strategy and were subcloned, overexpressed and purified in the same way as the wild-type proteins.

Protein crystallization. The hanging-drop vapour-diffusion method was performed at room temperature during crystallization. DltB and DltC proteins were purified as mentioned above, and crystals were obtained from DltB purified with *n*-nonyl-β-D-glucopyranoside (Anatrace). For crystallization of the DltB–DltC complex, DltB and DltC were purified separately and mixed before crystallization at a molar ratio of 1:2. Crystals belonging to crystal form I (space group $P2_1$, Extended Data Table 1) were crystallized in buffer containing 21% PEG400, 100 mM Tris-HCl pH 7.5, 100 mM NaCl and 100 mM $MgCl_2$. Crystals belonging to crystal form II (space group $P2_1$, Extended Data Table 1) were crystallized in buffer containing 27% PEG400, 100 mM sodium citrate pH 5.6, 200 mM $NH_4H_2PO_4$ and 100 mM $(NH_4)_2SO_4$. Crystals belonging to crystal form III (space group $P2_12_12_1$, Extended Data Table 1) were crystallized in buffer containing 27% PEG400, 100 mM HEPES pH 7.5, 200 mM sodium citrate tribasic dihydrate and 3% 1,5-diaminopentane dihydrochloride. For crystals in the different crystal forms above, thin or thick rod-shaped crystals typically grew for 1 to 2 weeks before reaching full crystal size. Gold derivatives were obtained by soaking the crystals in crystal form I for 2 h in mother liquor containing 2 mg ml^{-1} $KAu(CN)_2$.

Data collection and structure determination. The crystals were directly flash-frozen in liquid nitrogen. Screening and data collection were performed at the Advanced Light Source, beamlines 5.0.1, 8.2.1 and 8.2.2. All diffraction data were processed by HKL2000[31]. The single-wavelength anomalous dispersion (SAD) dataset was collected near the gold L-III absorption edge at a wavelength of 1.02 Å (Extended Data Table 1). The gold derivative sites and the initial phases were determined by PHENIX[32]. Twenty gold derivative sites were found in one asymmetric unit, and the experimental electron density map clearly showed the presence of four DltB molecules in one asymmetric unit. The *B. subtilis* DltC crystal structure (PDB ID: 4BPH) was used as the searching model for our DltC molecules[33]. The complex model was improved using iterative cycles of manual rebuilding with the program Coot[34] and refinement with a native dataset of 3.30 Å using Refmac5 of the CCP4 7.0 program suite[35]. The structures for crystal forms II and III were solved by molecular replacement using the model from crystal form I. All structure model figures in the paper were generated using PyMOL[36]. The protein conservation surface was generated using the ConSurf server[37], based on the alignment of DltB sequences generated using T-Coffee[38].

Binding assay. Pull-down assays were performed as described below. Twenty micrograms of wild-type DltB (or DltB mutants), 10 μg of wild-type GST–DltC (or GST–DltC mutants) and 10 μl GS4B resin were mixed in 100 μl of pull-down buffer containing 25 mM HEPES pH 7.5, 150 mM NaCl and 0.15% (w/v) *n*-decyl-β-D-maltopyranoside. The mixed samples were incubated at 4 °C on a rotisserie for 1 h, followed by washing the resin with pull-down buffer three times. During each wash, 100 μl of pull-down buffer was added to each sample and the solution was incubated at room temperature for 2 min before centrifugation and removal of supernatant. After washing, the resin samples were analysed by SDS–PAGE with Coomassie blue staining.

Binding assays were also performed at room temperature using the Octet system (FortéBio). Free GST, and GST-tagged wild-type DltC or DltC mutants were mobilized on anti-GST biosensors (FortéBio). After quenching with free GST to block free antibody sites on the biosensors, the biosensors were dipped into DltB solutions for binding measurements. The concentration gradient of DltB used in the Octet binding assay is: 0.03 μM, 0.1 μM, 0.3 μM, 1 μM, 3 μM, 10 μM.

Construction of *B. subtilis* strain for functional assays. The *cat* gene was amplified by PCR from pGEMcat, and 500 bp upstream and downstream of *dlt* operon fragments were amplified from the *B. subtilis* genome. These three pieces were assembled using isothermal assembly and transformed directly into the *B. subtilis* HM1 strain, resulting in *dlt*-operon-deleted *B. subtilis* (Δ*dlt*). The deletion was confirmed by PCR amplification and Sanger sequencing.

The natural *dlt* locus was amplified and cloned into pMMB752. Mutations of the *dltB* gene in pMMB752 carrying the *dlt* operon and Flag-tagged constructs were generated on the basis of a standard PCR method, followed by isothermal assembly to ligate the ends together. The pMMB752 constructs were transformed into *B. subtilis* with the *dlt* operon deleted from its native locus to generate strains for use in assays. Cells used here and in the following functional experiments were cultured in the presence of appropriate antibiotics to avoid possible contamination.

Detection of LTA D-alanylation. This assay was established on the basis of a previously reported method[14]. Wild-type *B. subtilis* HM1 strain, and *dlt*-operon-deleted *B. subtilis* HM1 strain complemented with either empty pMMB752 vector or vectors containing natural *dlt*-operon-bearing mutations on the *dltB* gene (untagged or Flag-tagged), were inoculated from fresh colonies on plate into liquid LB medium supplemented with 0.5 μg ml^{-1} erythromycin. Overnight cultures were diluted into 3 ml of LB at an OD_{600} of 0.1 and grown to an OD_{600} of 0.6. Cells were pelleted and resuspended into 1.5 ml of assay medium containing 0.25× LB, 50 mM Bis-Tris pH 6.0, and 200 μg ml^{-1} D-cycloserine. To test the inhibition of *m*-AMSA on LTA D-alanylation for wild-type *B. subtilis*, a final concentration of 150 μM of *m*-AMSA (Abcam) was supplemented into the assay medium. After incubation in the assay medium for 30 min, ^{14}C-D-alanine (Moravek Biochemicals) was added to a final concentration of 25 μM for an additional incubation of 30 min or 120 min. Cells were pelleted and resuspended with SDS-loading buffer, followed by a freeze–thaw cycle. Samples were vortexed and boiled for 5 min before loading onto 4–20% gradient Tris/glycine gel (Bio-Rad). Gels were dried and exposed to a phosphor storage screen for 3 days before imaging with Typhoon FLA 9000 gel imaging scanner (GE Healthcare).

To compare the expression level of C-terminal Flag-tagged DltB in corresponding *B. subtilis* strains, each strain was cultured in 1 l LB to OD_{600} of 0.6. Cells were collected and disrupted by French press, and the cell membrane was isolated by ultracentrifugation after removing cell debris by low-speed centrifugation. The membrane of each strain was resuspended with buffer containing 25 mM Tris-HCl 8.0, 150 mM NaCl into 500 μl, followed by freezing at −80 °C. One microlitre of each membrane sample was run onto SDS–PAGE and the expression of Flag-tagged DltB was detected by western blotting.

Survival assays. *Dlt* knockout strains of the Gram-positive bacterium *B. subtilis* are sensitive to the cell-wall-degrading enzyme lysozyme[39]. *B. subtilis* strains were struck on LB plates (supplemented with the appropriate antibiotic when needed) from freezer stocks and incubated overnight at 37 °C. The resulting growth on plates was used to inoculate 2-ml LB broth cultures in glass tubes. The cultures were grown at 37 °C with shaking (260 r.p.m.) to an OD_{600} of 1.0–2.0. All of the cultures were adjusted to an OD_{600} of 0.3 and then serially diluted in LB broth with tenfold dilutions. For each strain, 5 μl of each dilution was plated onto LB plates and LB plates supplemented with 30 μg ml^{-1} of lysozyme (Fisher) and incubated at 30 °C overnight. After incubation, colonies were enumerated and plates were imaged with a Bio-Rad Gel Doc XR+ Molecular Imager.

Reporting summary. Further information on research design is available in the Nature Research Reporting Summary linked to this paper.

Data availability

Atomic structures have been deposited in the Protein Data Bank (PDB) with accession codes 6BUG (crystal form I), 6BUH (crystal form II) and 6BUI (crystal form III). All other data that support the findings of this study are available from the corresponding author upon reasonable request.

31. Otwinowski, Z. & Minor, W. Processing of X-ray diffraction data collected in oscillation mode. *Methods Enzymol.* **276**, 307–326 (1997).
32. Adams, P. D. et al. PHENIX: a comprehensive Python-based system for macromolecular structure solution. *Acta Crystallogr. D* **66**, 213–221 (2010).
33. Zimmermann, S. et al. High-resolution structures of the D-alanyl carrier protein (Dcp) DltC from *Bacillus subtilis* reveal equivalent conformations of apo- and holo-forms. *FEBS Lett.* **589**, 2283–2289 (2015).
34. Emsley, P., Lohkamp, B., Scott, W. G. & Cowtan, K. Features and development of Coot. *Acta Crystallogr. D* **66**, 486–501 (2010).
35. Collaborative Computational Project, Number 4. The CCP4 suite: programs for protein crystallography. *Acta Crystallogr. D* **50**, 760–763 (1994).
36. Delano, W. L. & Brünger, A. T. Helix packing in proteins: prediction and energetic analysis of dimeric, trimeric, and tetrameric GCN4 coiled coil structures. *Proteins* **20**, 105–123 (1994).
37. Ashkenazy, H. et al. ConSurf 2016: an improved methodology to estimate and visualize evolutionary conservation in macromolecules. *Nucleic Acids Res.* **44**, W344–W350 (2016).
38. Taly, J. F. et al. Using the T-Coffee package to build multiple sequence alignments of protein, RNA, DNA sequences and 3D structures. *Nat. Protoc.* **6**, 1669–1682 (2011).
39. Guariglia-Oropeza, V. & Helmann, J. D. *Bacillus subtilis* σ^V confers lysozyme resistance by activation of two cell wall modification pathways, peptidoglycan *O*-acetylation and D-alanylation of teichoic acids. *J. Bacteriol.* **193**, 6223–6232 (2011).

a

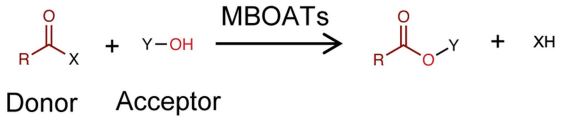

b

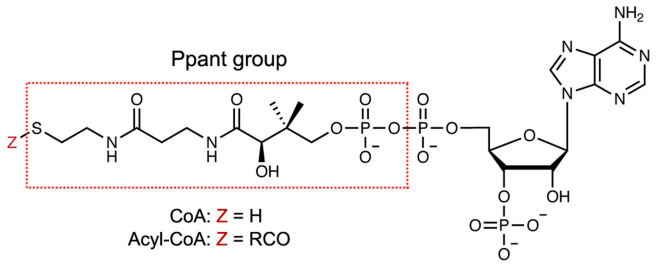

c

MBOAT	Acyl-group Donor	Acyl-group Acceptor
Porcupine	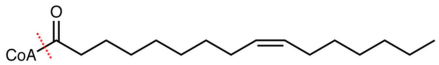	Wnt-Ser209-OH
GOAT	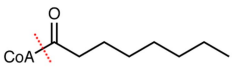	Ghrelin-Ser3-OH
DGAT1	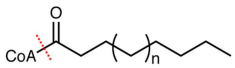	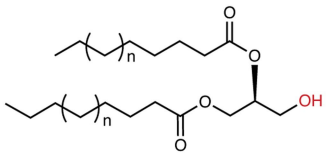 Diacylglycerol
ACAT	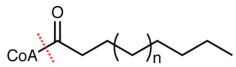	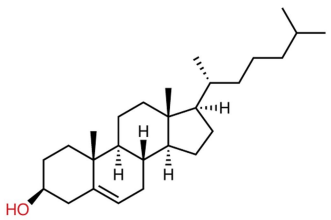 Cholesterol
DltB	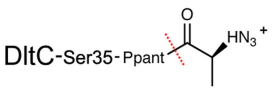	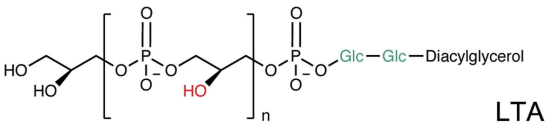 LTA

d

Extended Data Fig. 1 | MBOAT-catalysed reactions and chemical structures of MBOAT substrates. a, General reaction catalysed by MBOATs. **b**, Structure of CoA and acyl-CoA. The red rectangle highlights the Ppant prosthetic group within the CoA structure. For known acyl-group donors of MBOATs, the acyl groups are covalently linked with a sulfhydryl group (for example, that of Ppant in acyl-CoA or DltC-Ppant). **c**, Comparison of acyl-group donors and acceptors of PORCN, GOAT, DGAT1, ACAT and DltB. In the acyl-group donor column, the red dashed lines indicate the bonds that are broken during acyl-transfer reactions. In the acyl-group acceptor column, the hydroxyl groups that accept acyl groups are highlighted in red. ACAT1, ACAT2 and DGAT1 use saturated and unsaturated long-chain acyl-CoA. **d**, The reaction catalysed by DltB. DltB catalyses D-alanylation of both wall teichoic acid and LTA. Because the D-alanylation of wall teichoic acid is at least partially dependent on LTA D-alanylation, here we discuss only the D-alanylation of LTA. DltB transfers D-alanyl groups onto hydroxyl groups of the polyglycerolphosphate chain of the LTA molecule. For simplicity, only the type I LTA structure is shown here. The fatty-acid chains are responsible for the anchoring of LTA to the membrane of Gram-positive bacteria.

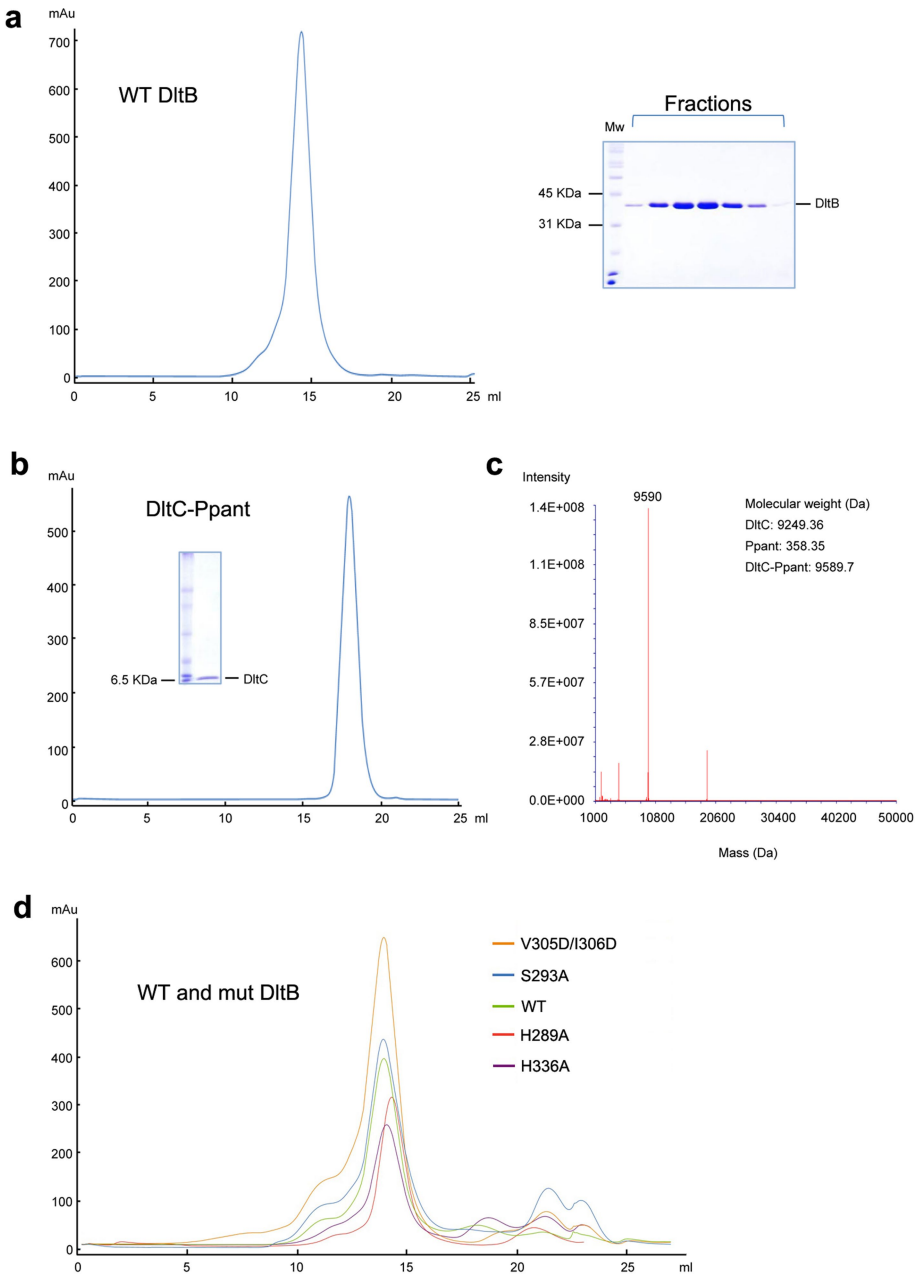

Extended Data Fig. 2 | Purification of DltB, DltC-Ppant and DltB mutants. a, SEC profile of DltB. DltB can be purified to homogeneity in most detergents and is well-behaved during SEC. **b**, SDS–PAGE and SEC profile of DltC. **c**, Mass spectrometry analysis of DltC species. This indicates that purified DltC has a molecular mass of 9,590 Da, which is equal to the calculated molecular mass of Ppant-modified DltC, referred to as DltC-Ppant. **d**, SEC profile of wild-type and mutant DltB proteins. DltB mutants including V305D/I306D, S293A, H289A and H336A are properly folded, as they migrate predominantly as a monomeric peak, similar to wild-type DltB.

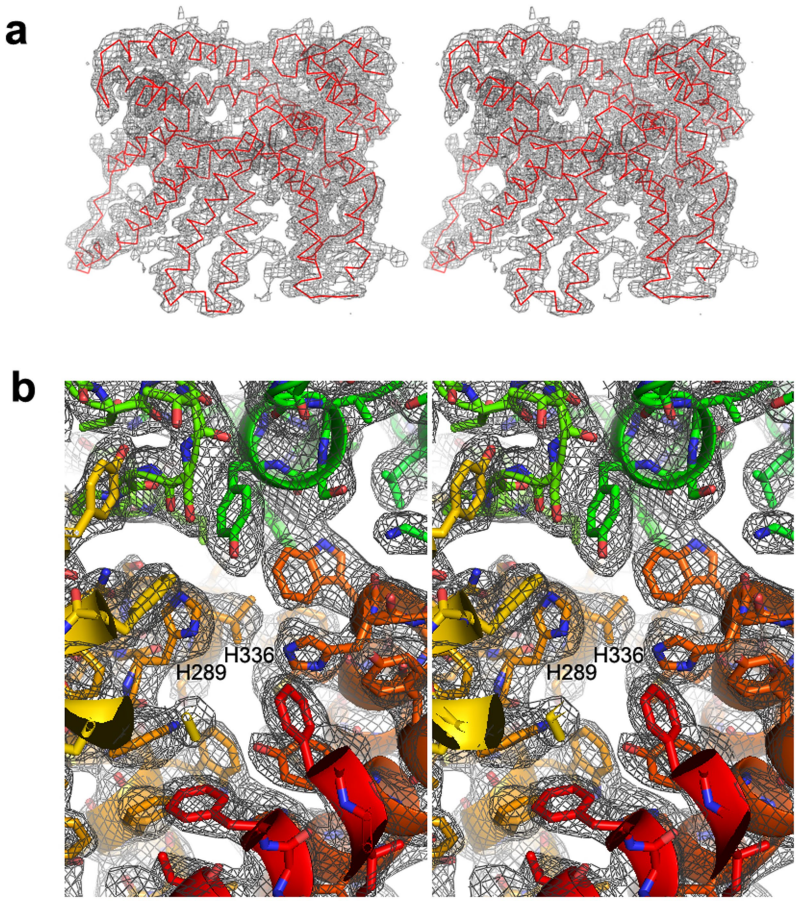

Extended Data Fig. 3 | Electron density map of DltB. a, Stereo experimental electron density map, using phases derived from an Au-SAD phasing (Extended Data Table 1). This $2F_o–F_c$ map is contoured at 1.0σ. DltB backbone tracing is shown in red. **b**, The final $2F_o–F_c$ electron density map of the crystal form II (Extended Data Table 1). This map is contoured at 1.0σ, shown in stereo and in an orientation approximately looking down the funnel. The catalytic His336 as well as His289 (another conserved residue (either His or Asn) among MBOAT proteins) are labelled. Both His336 and His289 are located at the bottom of the extracellular funnel, and sandwich the top opening of the transmembrane tunnel.

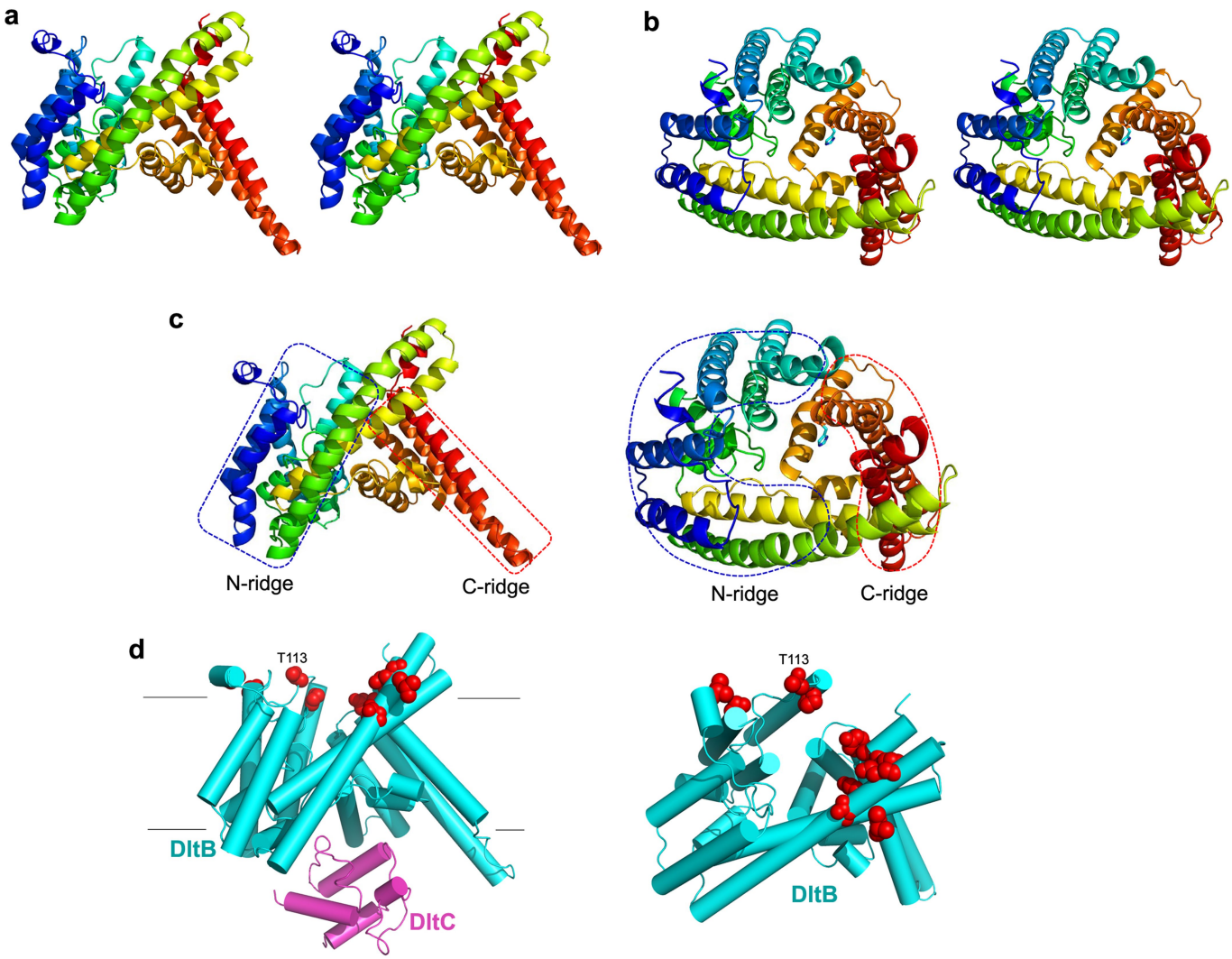

Extended Data Fig. 4 | Stereo view of DltB structure, and an extracellular 'ring' of DltB residues associated with a switch of pathogen host. a, The 'front' side view of DltB (stereo view is provided). **b**, The 'top' view of DltB, looking from the extracellular space (stereo view is provided). The His336 side chain is shown as sticks. The extracellular funnel is clear at this angle. **c**, Cartoon illustration of the N- and C-ridges of DltB in two orthogonal views. **d**, Locations of pathogen-host-sensitive sites in *S. aureus* DltB (I2, V61, T113, H121, I227, Q231, Y247, Y250, Y346, G401 and K402) are labelled with red balls in corresponding residues of the *S. thermophilus* DltB structure. It is clear that all 11 sites are located at the apex of the extracellular ridge of DltB. *S. aureus* DltB T113 is not conserved and does not have a corresponding residue in other DltBs (see Extended Data Fig. 5): here, the position of its closest residue is labelled. The intracellular DltC is shown in magenta. The DltB structure in these two panels are related with a 45° rotation.

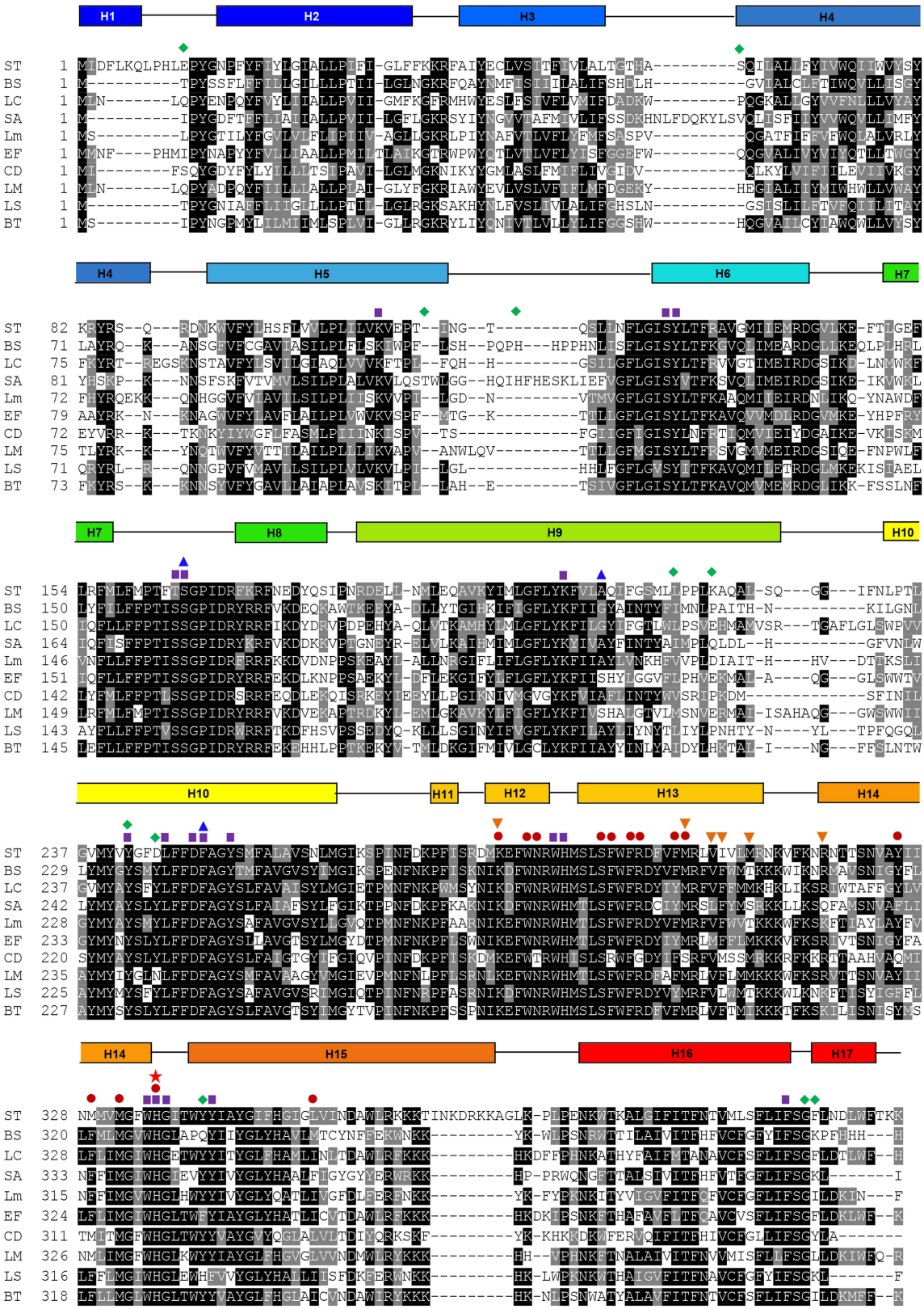

Extended Data Fig. 5 | DltB sequence alignment. DltB sequences of representatives from 10 different genera of Gram-positive bacteria were chosen for sequence alignment using the T-Coffee server. Secondary structural elements of DltB are indicated above the alignment. Residues that form the funnel are identified by purple squares, and residues that form the tunnel are identified with dark red dots. DltB residues involved in direct interaction with DltC are indicated with orange inverted triangles. Residues corresponding to the three sites for which single-point mutations desensitize *S. aureus* to inhibition by *m*-AMSA are indicated with blue triangles. Residues of *S. aureus* DltB, the mutation of which alter the host preference from being human-specific to being capable of infecting rabbits, are indicated with green diamonds. A red star highlights the histidine residue that is completely conserved among MBOATs. ST, *S. thermophilus*; BS, *B. subtilis*; LC, *L. casei*; SA, *S. aureus*; Lm, *Listeria monocytogenes*; EF, *Enterococcus faecalis*; CD, *Clostridioides difficile*; LM, *Leuconostoc mesenteroides*; LS, *Lysinibacillus sphaericus*; BT, *Brochothrix thermosphacta*.

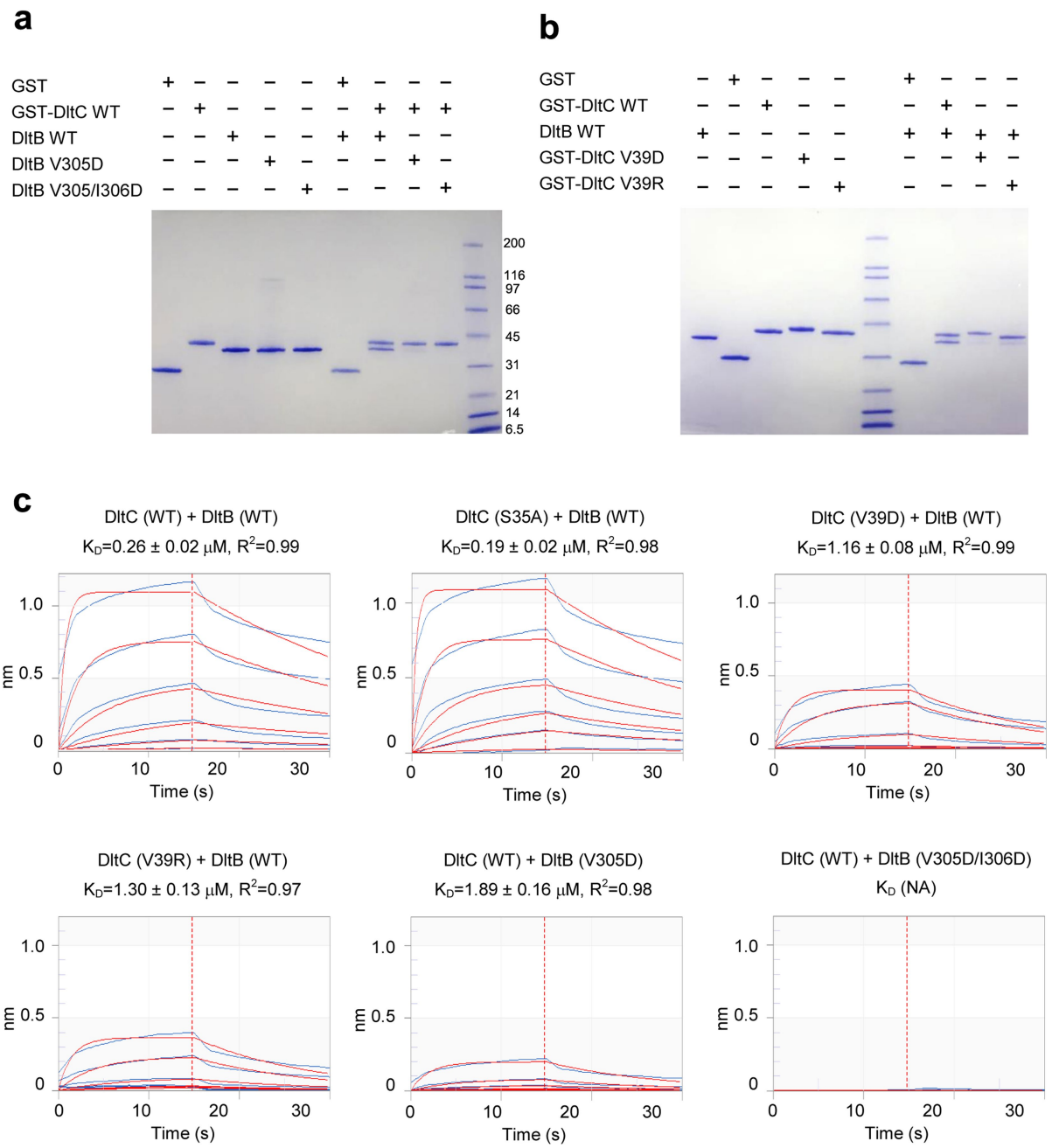

d

Samples in Octet Assay		K_D (μM)
GST-DltC	DltB	
WT	WT	0.26 ± 0.02
S35A	WT	0.19 ± 0.02
V39D	WT	1.16 ± 0.08
V39R	WT	1.30 ± 0.13
WT	V305D	1.89 ± 0.16
WT	V305D/I306D	NA

Extended Data Fig. 6 | See next page for caption.

Extended Data Fig. 6 | GST pull-down and Octet assays for analysis of the interaction between DltB and DltC-Ppant. a, Results of using wild-type GST–DltC to pull-down either wild-type or mutant DltB, with GST to pull-down wild-type DltB as a negative control. Lanes 1–5 show inputs in this experiment. Pull-down results demonstrate that DltB and DltC can form a stable complex at an almost 1:1 molar ratio. DltB(V305D) loses most of its capacity to bind to wild-type GST–DltC, whereas the binding between DltB and DltC was completely abolished with the double mutant DltB(V305D/I306D). **b**, Results of using wild-type or mutant GST–DltC to pull-down wild-type DltB. Lanes 1–5 show inputs in this experiment. The mutant GST–DltC(V39D) runs slightly slower than wild-type GST–DltC and GST–DltC(V39R) on SDS–PAGE. Both GST–DltC(V39D) and GST–DltC(V39R) lost most of their capacity to bind with wild-type DltB. Pull-down experiments were performed at least twice technically, with the same results. **c**. Binding-affinity measurements for DltB and DltC using the Octet technique. Wild-type GST–DltC-Ppant and GST–DltC(S35A) show similar binding affinities with wild-type DltB. Data are shown in blue, with the corresponding fits in red. The DltB concentration gradient used here is: 0.03 μM, 0.1 μM, 0.3 μM, 1 μM, 3 μM, 10 μM. Octet assays were performed twice technically. **d**, Summary of Octet binding assay. Wild-type DltC and GST–DltC(S35A) show similar binding affinities to wild-type DltB. Mean K_d values and s.d. are shown for each assay. Mutation of residues on the binding surface of either DltB or DltC can reduce or abolish their binding.

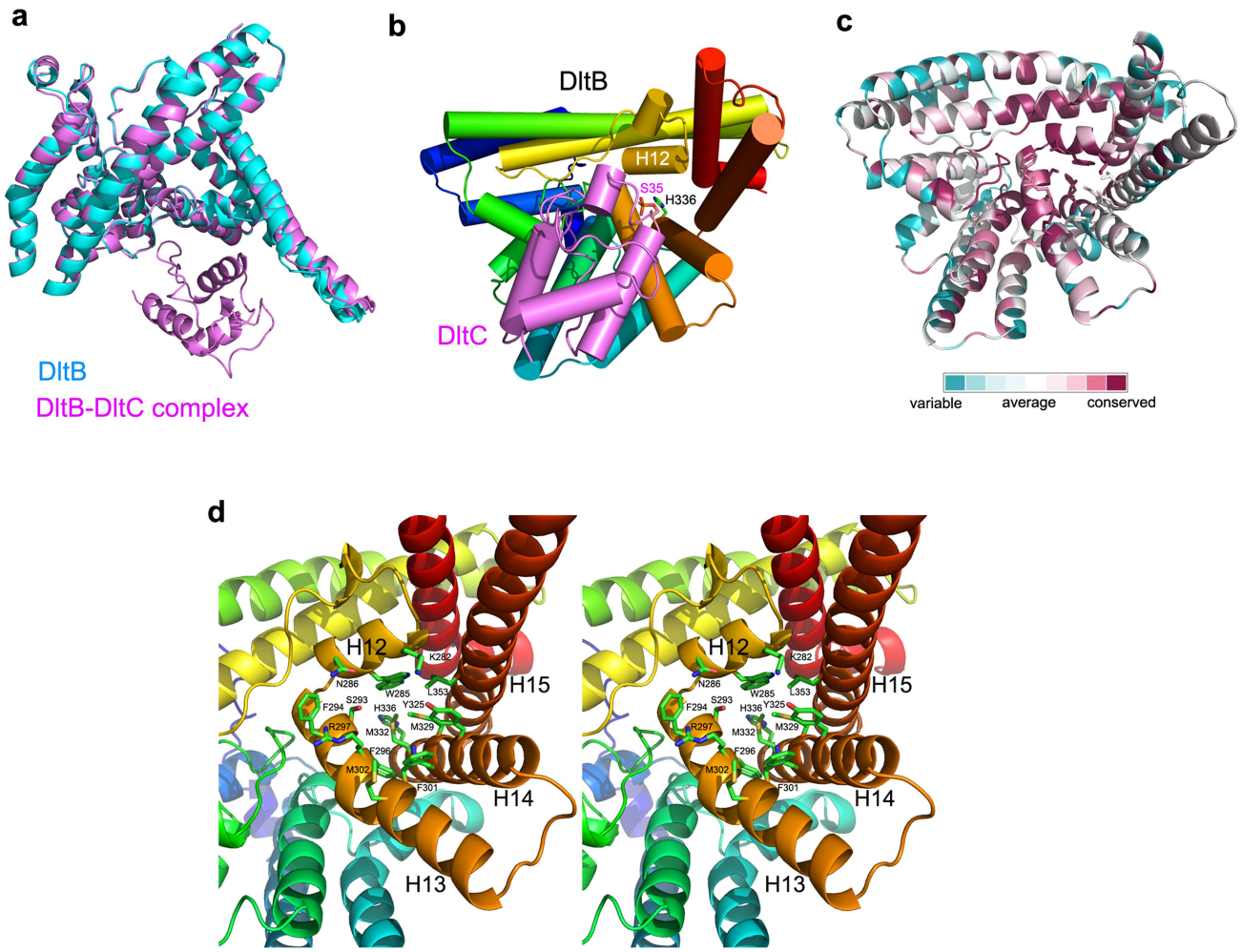

Extended Data Fig. 7 | Structural details of the DltB–DltC interface and the DltB tunnel. a, Superposition of crystal structures of DltB and the DltB–DltC complex. There is no significant conformational change in DltB upon the binding of DltC-Ppant. **b**, Cylinder illustration of the DltB–DltC-Ppant complex, viewed from the bottom of the DltB tunnel. DltB is coloured in rainbow, with DltC in purple. **c**, Conservation of the DltB tunnel region. Residues involved in tunnel formation are also highly conserved among DltB proteins from different species (Extended Data Fig. 5). **d**, Stereo view of the DltB tunnel and residues forming this tunnel. The tunnel is formed by three helices from the C-ridge (H13, H14 and H15) and the short H12 helix. Residues involved in tunnel formation in our structures are: Lys282, Trp285, Asn286, Ser293, Phe294, Phe296, Arg297, Phe301, Met302, Tyr325, Asn328, Met329, Met332, Leu353, and His336 (which is also involved in the formation of extracellular funnel).

a

Corresponding residues in two species	
S. thermo-philus	*B. subtilis*
H289A	H281A
S293A	S285A
H336A	H328A
V305D/ I306D	V297D/ F298D

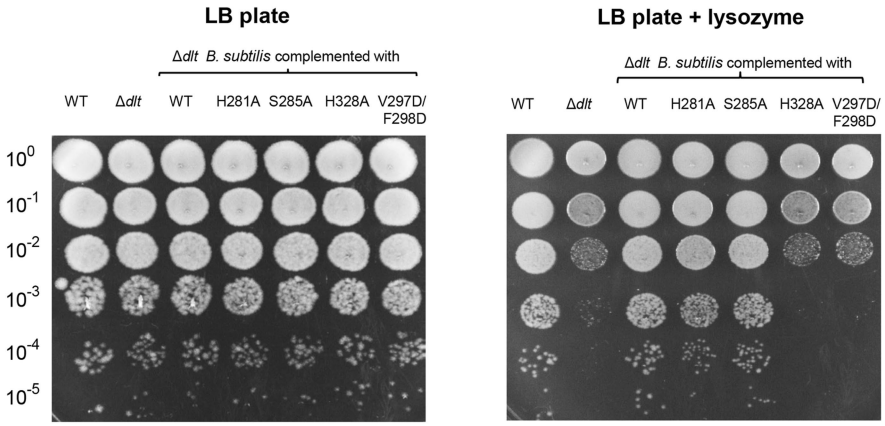

b

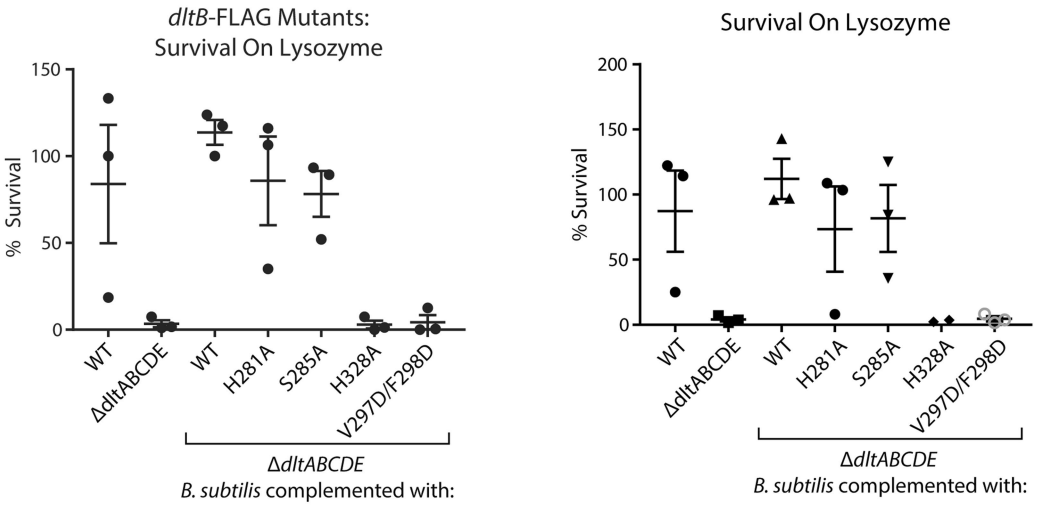

c

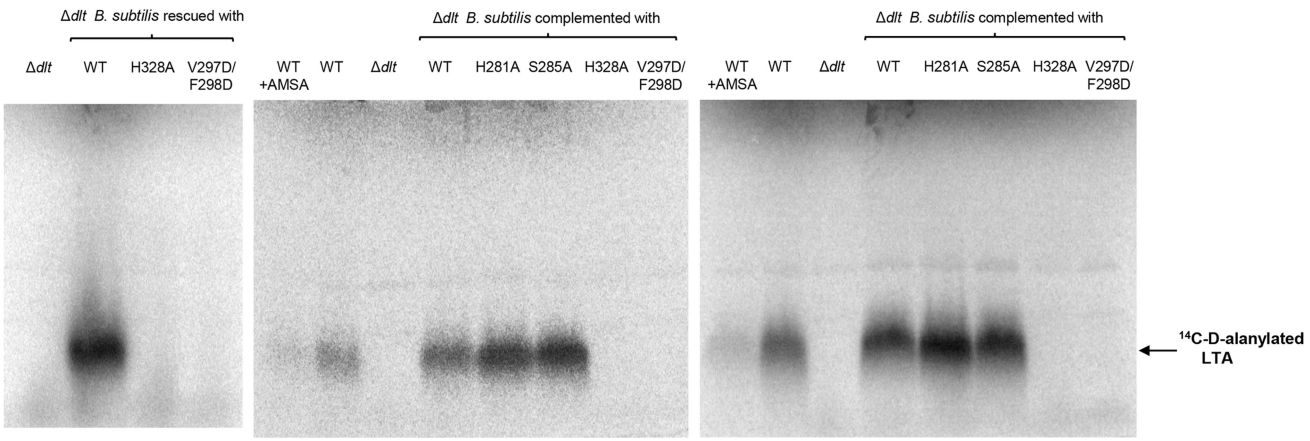

Extended Data Fig. 8 | See next page for caption.

Extended Data Fig. 8 | Survival and LTA D-alanylation assays for wild-type and mutant DltB. a, Lysozyme susceptibility survival assay. For DltB residues used in both LTA D-alanylation and survival assays, corresponding DltB residue numbers in two species are listed. The endogenous *dlt* operon was deleted in the *B. subtilis* strain and complemented with an ectopic copy of the wild-type *dlt* operon without tag on DltB. Representative images of serial dilutions of cells plated on LB agar (left) and LB agar supplemented with 30 μg ml^{-1} of lysozyme (right). The genotype of the *dltB* gene is indicated above the corresponding column of serial dilutions. Dilutions of cells are indicated on the *y* axis. Mutation of the critical histidine (His328) and residues of DltB involved in binding with DltC(V297/F298) increase the susceptibility to lysozyme of *B. subtilis*. **b**, Per cent survival of *B. bacillus* variants towards lysozyme treatment. This was calculated by dividing the colony-forming units (CFUs) from lysozyme plates by the CFUs from LB-only plates. Data are mean ± s.d. of three biological replicates. The genotype of *dltB* is indicated at the bottom. *B. subtilis* strains containing untagged DltB show a similar lysozyme susceptibility pattern to those containing Flag-tagged DltB. **c**, LTA D-alanylation assay. In experiment 1, the assay time was 120 min after ^{14}C-D-alanine was added, whereas for experiments 2 and 3, the assay time was 30 min. Experiments 2 and 3 are two parallel assays for LTA D-alanylation detection. AMSA represents *m*-AMSA, a DltB inhibitor.

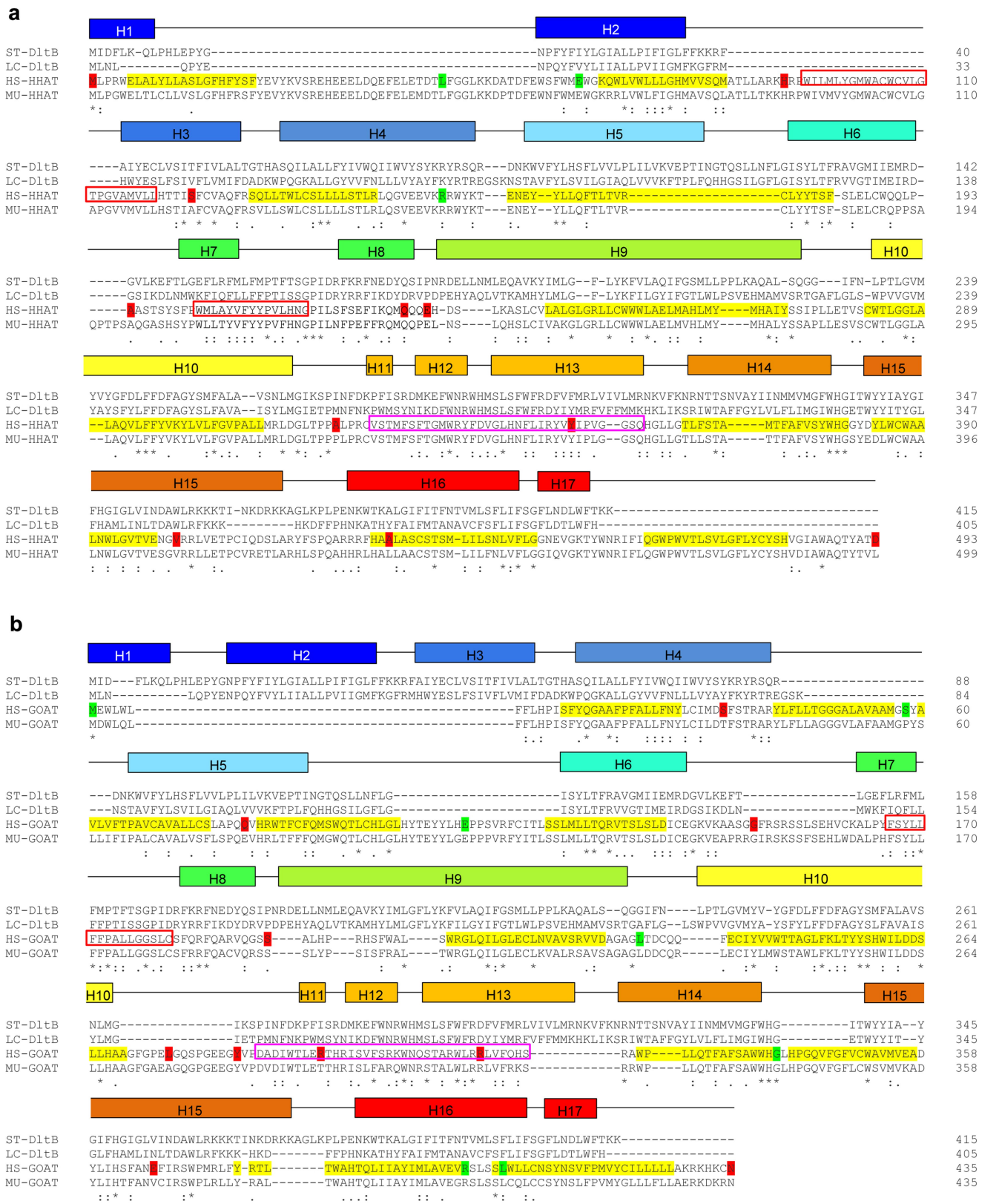

Extended Data Fig. 9 | Comparison and rationalization of topological data. a, Comparison of HHAT topology data with the DltB structure. **b**, Comparison of GOAT topology data with the DltB structure. In both panels, secondary structures above DltB sequences are generated from our DltB crystal structure. Reported topology assignments of HHAT and GOAT were achieved using human proteins. Here we highlighted the predicted HHAT or GOAT transmembrane helices for each protein with yellow background within sequences. Residues for human HHAT and GOAT that were experimentally verified to be located on the cytoplasmic side are coloured in red, and residues which are on the lumenal side are coloured in green. Helices and/or loops that are predicted to be associated with the membrane surface or buried halfway within the membrane on the cytoplasmic side are indicated with red and magenta rectangles, respectively. It is clear that the regions corresponding to DltB H7–H14 are topologically more conserved than those forming the DltB N- and C-ridges.

Extended Data Table 1 | Data collection, phasing and refinement statistics

Data collection	Crystal form I		Crystal form II	Crystal form III
	Au-SAD	Native	Native	Native
Space group	$P2_1$	$P2_1$	$P2_1$	$P2_12_12$
Content per ASU	4 DltB + 3 DltC(Ppant)		4 DltB + 4 DltC(Ppant)	4 DltB
Wavelength (Å)	1.02	1.00	1.00	1.00
Temperature (K)	100	100	100	100
Cell dimensions				
a, *b*, *c* (Å)	109.3, 122.0, 126.3	108.7, 121.1, 126.5	108.7, 124.6, 126.7	140.2, 242.1, 96.2
α, β, γ (°)	90, 101.1, 90	90, 101.6, 90	90, 97.0, 90	90, 90, 90
Resolution (Å)	3.80 (3.87-3.80)	50.0-3.30 (3.40-3.30)	50.0-3.15 (3.24-3.15)	50.0-3.30 (3.40-3.30)
R_{sym}	0.152 (1.450)	0.170 (1.661)	0.165 (0.929)	0.115 (1.203)
$I/\sigma(I)$	19.0 (1.3)	13.1 (1.2)	8.6 (1.2)	11.5 (1.4)
$CC_{1/2}$	(0.626)	(0.732)	(0.582)	(0.563)
Completeness (%)	99.9 (99.4)	99.5 (98.7)	98.5 (87.8)	97.5 (98.1)
Redundancy	7.2 (6.5)	6.4 (6.3)	3.6 (2.9)	3.8 (3.2)
Refinement				
Resolution (Å)		50.0-3.30	50.0-3.15	50.0-3.30
No. reflections		46614	54118	47040
R_{work} / R_{free}		0.289 / 0.311	0.276 / 0.299	0.280 / 0.300
No. atoms				
Protein		15679	16308	13792
Ligand/ion		0	0	0
Water		0	0	0
B-factors				
Protein		86.6	45.1	108.9
Ligand/ion		N/A	N/A	N/A
Water		N/A	N/A	N/A
R.m.s. deviations				
Bond lengths (Å)		0.009	0.009	0.009
Bond angles (°)		1.409	1.338	1.400
Ramachandran plot				
Most favored (%)		94.9	96.6	96.1
Allowed (%)		5.1	3.4	3.9
Disallowed (%)		0	0	0

Every diffraction dataset was collected from a single crystal. Values in parentheses are for highest-resolution shell.

nature research

Corresponding author(s): Wenqing Xu

Reporting Summary

Nature Research wishes to improve the reproducibility of the work that we publish. This form provides structure for consistency and transparency in reporting. For further information on Nature Research policies, see Authors & Referees and the Editorial Policy Checklist.

Statistical parameters

When statistical analyses are reported, confirm that the following items are present in the relevant location (e.g. figure legend, table legend, main text, or Methods section).

n/a	Confirmed
☐	☒ The exact sample size (*n*) for each experimental group/condition, given as a discrete number and unit of measurement
☐	☒ An indication of whether measurements were taken from distinct samples or whether the same sample was measured repeatedly
☐	☒ The statistical test(s) used AND whether they are one- or two-sided *Only common tests should be described solely by name; describe more complex techniques in the Methods section.*
☒	☐ A description of all covariates tested
☒	☐ A description of any assumptions or corrections, such as tests of normality and adjustment for multiple comparisons
☐	☒ A full description of the statistics including central tendency (e.g. means) or other basic estimates (e.g. regression coefficient) AND variation (e.g. standard deviation) or associated estimates of uncertainty (e.g. confidence intervals)
☒	☐ For null hypothesis testing, the test statistic (e.g. *F*, *t*, *r*) with confidence intervals, effect sizes, degrees of freedom and *P* value noted *Give P values as exact values whenever suitable.*
☒	☐ For Bayesian analysis, information on the choice of priors and Markov chain Monte Carlo settings
☒	☐ For hierarchical and complex designs, identification of the appropriate level for tests and full reporting of outcomes
☒	☐ Estimates of effect sizes (e.g. Cohen's *d*, Pearson's *r*), indicating how they were calculated
☐	☒ Clearly defined error bars *State explicitly what error bars represent (e.g. SD, SE, CI)*

Our web collection on statistics for biologists may be useful.

Software and code

Policy information about availability of computer code

Data collection	Beamline Operating Software (BOS)
Data analysis	PHENIX (phase determination), COOT (model building), CCP4 (structure refinement), PyMOL (structure analysis and structure related figures preparation), ConSurf server (protein surface conservation pattern generation), T-Coffee server (protein sequence alignment).

For manuscripts utilizing custom algorithms or software that are central to the research but not yet described in published literature, software must be made available to editors/reviewers upon request. We strongly encourage code deposition in a community repository (e.g. GitHub). See the Nature Research guidelines for submitting code & software for further information.

Data

Policy information about availability of data

All manuscripts must include a data availability statement. This statement should provide the following information, where applicable:

- Accession codes, unique identifiers, or web links for publicly available datasets
- A list of figures that have associated raw data
- A description of any restrictions on data availability

Atomic structures have been deposited in the Protein Data Bank (PDB) with accession codes 6BUG (crystal form I), 6BUH (crystal form II) and 6BUI (crystal form III). All other data that support the findings of this study are available from the corresponding author upon reasonable request.

Field-specific reporting

Please select the best fit for your research. If you are not sure, read the appropriate sections before making your selection.

☒ Life sciences ☐ Behavioural & social sciences ☐ Ecological, evolutionary & environmental sciences

For a reference copy of the document with all sections, see nature.com/authors/policies/ReportingSummary-flat.pdf

Life sciences study design

All studies must disclose on these points even when the disclosure is negative.

Sample size	Each X-ray diffraction dataset was collected with a single crystal until decent data redundancy is reached.
Data exclusions	Exclusion of X-ray diffraction outliers was done using the program HKL2000, based on standard criteria. No data exclusions for biochemical assays.
Replication	To ensure reproducibility of experimental findings, all biochemical assays were performed at least twice to confirm the results. All attempts at replication were successful.
Randomization	5% of diffraction data was randomly selected by the CCP4 program for calculation of R free.
Blinding	Blinding was not used. We used bacteria for in vivo studies and every experiment was replicated to confirm the results. Two different sets of functional assays (LTA D-alanylation and survival assays) were performed by different authors and the results were consistent with each other.

Reporting for specific materials, systems and methods

Materials & experimental systems

n/a	Involved in the study
☒	☐ Unique biological materials
☐	☒ Antibodies
☒	☐ Eukaryotic cell lines
☒	☐ Palaeontology
☒	☐ Animals and other organisms
☒	☐ Human research participants

Methods

n/a	Involved in the study
☒	☐ ChIP-seq
☒	☐ Flow cytometry
☒	☐ MRI-based neuroimaging

Antibodies

Antibodies used	FLAG Tag Monoclonal Antibody (FG4R) generated in mouse was purchased from Invitrogen (Catalog # MA1-91878) and was 1:1000 diluted while used for detection the expression of FLAG-tagged proteins in western blotting. HRP conjugated goat anti mouse secondary antibody was purchased from Invitrogen (Catalog # 62-6520) and 1:2000 diluted to recognize anti-FLAG primary antibody. Pierce™ ECL Western Blotting Substrate from Thermo Fisher Scientific (Catalog # 32106) was use for further detection of the protein bands. Anti-GST biosensors used in Octet assay were purchased from ForteBIO (Part No: 18-5096).
Validation	For anti-FLAG antibody (FG4R), it is stated on official website that antibody target was verified by cell treatment to ensure the antibody binds to the antigen. For anti-GST biosensors, binding between the biosensors and GST can be detected by Octet.